J Supercond Nov Magn (2017) 30:951–958
DOI 10.1007/s10948-016-3888-1

ORIGINAL PAPER

Electronic Structure, Phase Stability, and Elastic Properties of Inverse Heusler Compound Mn_2RuSi at High Pressure

Ting Song[1,2] · Jun-Hong Tian[2,3] · Qin Ma[1] · Xiao-Wei Sun[2] · Zi-Jiang Liu[2,4]

Received: 26 September 2016 / Accepted: 27 October 2016 / Published online: 8 November 2016

Abstract The structural, magnetic, electronic, and elastic properties of the new Mn-based Heusler alloy Mn_2RuSi at high pressure have been investigated using the first-principles calculations within density functional theory. Present calculations predict that Mn_2RuSi in stable $F\bar{4}3m$ configuration is a ferrimagnet with an optimized lattice parameter 5.76 Å. The total spin magnetic moment is 2.01 μ_B per formula unit and the partial spin moments of Mn (A) and Mn (B) which mainly contribute to the total magnetic moment are 2.48 and -0.66 μ_B, respectively. Mn_2RuSi exhibits half metallicity with an energy gap in the spin-down channels. The study of phase stability indicates that the elastic stiffness coefficients of Mn_2RuSi with $F\bar{4}3m$ structure satisfy the traditional mechanical stability restrictions until up to 100 GPa. In addition, various mechanical properties including bulk modulus, shear modulus, Young's modulus, and Poisson's ratio along with elastic wave velocitieshave also been obtained and discussed in details in the pressure range of 0–100 GPa based on the three principle elastic tensor elements C_{11}, C_{12}, and C_{44} for the first time.

Keywords Electronic structure · Phase stability · Elastic properties · Mn_2RuSi alloy · High pressure

1 Introduction

Full-Heusler alloys are ternary, magnetic, intermetallic compounds, usually containing Mn with $L2_1$ or XA crystal structures, and are defined by the generic formula X_2YZ, where X and Y are usually transition metals and Z is a group III, IV or V element. When the valence of X is larger than Y, crystallization of these compounds is reported in the well-known $L2_1$ structure with prototype Cu_2MnAl (the space group of $Fm\bar{3}m$ and the number of 225) and the atomic sequence is X-Y-X-Z. However, if the valence of the Y elements is the largest, the crystallization of these compounds are reported in the so-called XA structure, where the prototype is Hg_2CuTi and the atomic sequence is X-X-Y-Z (the space group of $F\bar{4}3m$ and the number of 216) [1]. The latter alloys are also known as inverse Heusler compounds. Compared with the Cu_2MnAl-type regular Heusler compounds, the Hg_2CuTi-type inverse Heusler compounds do not possess inversion symmetry, such that the Mn atoms in Mn_2RuSi become nearest neighbors, which leads to an antiparallel coupling of their magnetic moments. Inverse Heusler compounds are interesting for applications since they combine coherent growth on semiconductors with large Curie temperatures [2] and structural similarity relative to zinc-blend structure, which is suitable as spin injection source of semiconductor. Furthermore, they are considered to be potential shape memory alloy

✉ Qin Ma
maqin_lut@yeah.net

✉ Xiao-Wei Sun
sunxw_lzjtu@163.com

1 State Key Laboratory of Advanced Processing and Recycling of Non-ferrous Metals, Lanzhou University of Technology, Lanzhou, 730050, People's Republic of China

2 School of Mathematics and Physics, Lanzhou Jiaotong University, Lanzhou, 730070, People's Republic of China

3 Institute of Atomic and Molecular Physics, Sichuan University, Chengdu, 610065, People's Republic of China

4 Department of Physics, Lanzhou City University, Lanzhou, 730070, People's Republic of China

(SMA) due to the fully spin-polarized electrons at the Fermi level.

Since the discovery of half metallic properties [3], ferromagnetic shape memory effects (FSME) [4] and magnetic compensation behavior [5], Hg_2CuTi-type Mn_2-based Heusler alloys have attracted considerable attention in recent years Among them, new compounds Mn_2RuZ (Z = *s*, *p* elements) which contain a 4*d* element Ru have been synthesized by Endo et al [6]. They experimentally examined the structural and magnetic properties of new Mn_2RuZ (Z = Si, Sn) alloys and observed the glassy nature of these materials. The results are important, as we know, most Mn_2-based Heusler alloys are mainly composed of 3*d* transition metal elements, like as Mn_2VAl [7], Mn_2CoZ (Z = Al, Si, Ge, Sn, Sb) [3, 8, 9], Mn_2FeZ (Z = Al, Sb) [10], Mn_2CrZ (Z = Al, Ga, Si, Ge, Sb) [11], and Mn_2CuZ (Z = Si, Ge, Sb, Mg) [12–15]. The synthesis of Mn_2RuZ (Z = Si, Sn) enlarges the scope of exploring new functional materials in Heusler alloys. Recently, related theoretical studies have also been performed to investigate the half-metallic nature and the basic conclusions of half-metallic ferrimagnet with Hg_2CuTi-type structure for Mn_2RuSi have been obtained [16–18] Apart from these studies, no further theoretical or experimental information is available, especially the electronic and elastic properties under high pressure in the literature for $RuMn_2Si$ Heusler alloy. Following this, the present study has been conducted to predict the new half-metallic full-Heusler alloy $RuMn_2Si$ using the first-principles calculations within density functional theory. Electronic structure, phase stability, and elastic properties of Mn_2RuSi at high pressure have been investigated up to 100 GPa. In addition, various mechanical properties including bulk modulus (B), shear modulus (G), Young's modulus (E), and Poisson's ratio (σ) along with elastic wave velocities (V_m, V_s, and V_l) have also been obtained and discussed in detail with increasing ambient pressure conditions up to the considered pressures based on the three principle elastic tensor elements C_{11}, C_{12}, and C_{44} for Mn_2RuSi in stable $F\bar{4}3m$ configuration in the present work.

2 Computational Methodology

All of the first-principles calculations were carried out by the Cambridge Serial Total Energy Package (CASTEP) code [19]. The Vanderbilt ultrasoft pseudopotential method [20] within the generalized gradient approximation (GGA) of revised Perdew-Burke-Ernzerhof (PBEsol) [21] was adopted with the choices of $3d^5$ $4s^2$, $4s^2$ $4p^6$ $4d^7$ $5s^1$, and $3s^2$ $3p^2$ valence electrons for Mn, Ru, and Si atoms, respectively. The plane-wave cutoff energy was chosen to be 600 eV and it was adequate for the energy, structural, and electronic property calculations. The integrations over the Brillouin zone were replaced by discrete summation on special set of k points using Monkhorst-Pack scheme [22] and a mesh of 12 ×12 ×12 k points was employed for the selected Hg_2CuTi-type structure of Mn_2RuSi. The maximum magnitudes of the force on the atom, stress, and atomic position displacement between computational cycles were maintained below 0.01 eV/Å, 0.02 GPa, and 5 $\times 10^{-4}$ Å, respectively. The electronic wave functions were obtained by using the Pulay density-mixing scheme [23] for the self-consistent field calculation. The Broyden, Fletcher, Goldfarb, and Shannon (BFGS) quasi-Newton (variable-metric) minimization method [24] was applied to relaxing the whole crystal to reach the ground state configuration.

The elastic properties of Mn_2RuSi are explored by calculating their independent elastic constants C_{ij}, elastic stiffness coefficients c_{ij}, shear modulus G, bulk modulus B, Young's modulus E, Debye temperature θ_D, Poisson's ratio σ, and the compressional and shear wave velocities V_l and V_s, and related properties. Elastic constants are the measure of the shear and tensile strength of crystals in the long-wavelength limit. They are defined by means of a Taylor expansion of the total energy, $E\ (V,\ \delta)$, for the system with respect to a small strain δ of the lattice primitive cell volume V. The energy of a strained system is expressed as follows [25]:

$$E(V,\delta) = E(V_0,0) + V_0\left[\sum_i \tau_i\xi_i\delta_i + \frac{1}{2}\sum_{ij} C_{ij}\delta_i\xi_i\delta_j\right], \tag{1}$$

where $E\ (V_0,\ 0)$ is the energy of the unstrained system with equilibrium volume V_0, ξ_i is a factor to take care of Voigt index, and τ_i is an element in the stress tensor. Since the stress and strain tensors are symmetric, the 21 non-zero independent components for the general elastic stiffness tensors will reduce the number to 3 for Mn_2RuSi in stable cubic $F\bar{4}3m$ configuration. The elastic constants C_{11}, C_{12}, and C_{44} at different pressures are determined from the first-principles strain-stress relationships method. Both positive and negative strains are applied for each strain component, with a maximum strain value of 0.003, within which 6 distorted structures are generated.

In the following, we will introduce the formulas of other elastic moduli for the considered crystal system. From the calculated elastic constants, the bulk modulus B and shear modulus G for Mn_2RuSi alloy are obtained using the Voigt-Reuss-Hill (RVH) approximations [26–28], where subscript V denotes the Voigt bound, R denotes the Reuss bound, and H denotes the Hill average:

$$B = B_V = B_R = \frac{1}{3}(C_{11} + 2C_{12}), \tag{2}$$

$$G = G_H = \frac{G_R + G_V}{2}, \tag{3}$$

where

$$G_R = \frac{5C_{44}\,(C_{11} - C_{12})}{4C_{44} + 3\,(C_{11} - C_{12})}, \tag{4}$$

and

$$G_V = \frac{1}{5}\,(C_{11} - C_{12} + 3C_{44})\,. \tag{5}$$

The Young's modulus E can be given in terms of B and G by:

$$E = \frac{9BG}{3B + G}. \tag{6}$$

The ratio of the transverse compression to the longitudinal extension is called Poisson's ratio. The relation of Poisson's ratio σ with B and G is:

$$\sigma = \frac{3B - 2G}{2\,(3B + G)}. \tag{7}$$

The values of the shear sound velocity V_s and compressional sound velocity V_l can be calculated from Navier's equations [29],

$$V_s = \sqrt{\frac{G}{\rho}},\ V_p = \sqrt{\left(B + \frac{4}{3}G\right)\frac{1}{\rho}}, \tag{8}$$

and the average sound-wave velocity V_m can be computed using the following expression [30]:

$$V_m = \left[\frac{1}{3}\left(\frac{2}{V_s^3} + \frac{1}{V_p^3}\right)\right]^{-1/3}. \tag{9}$$

Then, the Debye temperature θ_D can be derived from the average sound velocity V_m and density ρ [29]:

$$\theta_D = \frac{h}{k}\left[\frac{3n}{4\pi}\left(\frac{N_A\rho}{M}\right)\right]^{1/3} V_m, \tag{10}$$

where h is the Planck's constant, k is the Boltzmann's constant, N_A is the Avogadro's number, n is the number of atoms per formula unit, and M is the molecular weight.

3 Results and Discussion

The X-ray powder data of the studied materials, reported by Endo et al. [6], reveal that under normal conditions, the Mn_2RuSi compound crystallizes in a Heusler-like cubic structure ($L2_1B$ or XA-type structure). The theoretical studies that were followed have been performed to investigate the site preference and the basic conclusions of half-metallic ferrimagnet with an inverse Heusler structure of XA type, i.e. Hg_2CuTi type rather than a disordered phase of $L2_1B$ type for Mn_2RuSi have been obtained [16–18]. For our studied compound Mn_2RuSi, Mn atoms occupy (0, 0, 0) and (0.25, 0.25, 0.25) sites, Ru atom enters at (0.5, 0.5, 0.5), and Z occupies (0.75, 0.75, 0.75) sites in Wyckoff coordinates in Hg_2CuTi-type structure. Two display styles in conventional cell and primitive cell which contains, respectively, 16 atoms and 4 atoms described above are presented in Fig. 1.

The structural optimization of Mn_2RuSi under high pressure is performed for the spin-polarized case. The pressure dependence of the normalized lattice constants a/a_0 and the normalized unit cell volume V/V_0 with pressure range from 0 to 100 GPa are illustrated in Fig. 2, where a_0 and V_0 are the zero-pressure equilibrium structure parameters. The calculated value of equilibrium lattice parameter in the present work is 5.76 Å, while the recent theoretical values are between 5.73 and 5.87 Å [16–18]. The experimental value is 5.826 Å [6]. Thus, our calculated lattice parameter matches well with the experimental and theoretical results, which indicates that the present calculations are reliable. From Fig. 2, it can be found that all the ratios decrease smoothly with pressure. By fitting the lattice parameter and volume curves, the following cubic function relationships for the GGA calculation can be obtained as:

$$\frac{a}{a_0} = 0.9998 - 0.0013P + 7.997\times10^{-6}P^2 - 2.806\times10^{-8}P^3, \tag{11}$$

$$\frac{V}{V_0} = 0.9993 - 0.0037P + 2.614\times10^{-5}P^2 - 9.419\times10^{-8}P^3. \tag{12}$$

The magnetic moment per formula unit for Mn_2RuSi can be determined from the number of the valence electrons using the Slater-Pauling rule [31] The total magnetic moment 2.01 μ_B obtained by present calculations is very close to integer value and agree well with the Slater-Pauling rule. Meanwhile, the spin-polarized calculations revealed that Mn_2RuSi possesses ferrimagnetic ground state and the partial spin moments of Mn (A) and Mn (B) which mainly contribute to the total magnetic moment are 2.48 and −0.66 μ_B, respectively. When pressure is up to 50 GPa, the total spin magnetic moment is 2.00 μ_B per formula unit and the partial spin moments of Mn (A) and Mn (B) are 2.02 and −0.20 μ_B, respectively. When pressure is up to 100 GPa, the total spin magnetic moment decreases slowly to 1.95 μ_B and the lattice parameter decreases to 5.333 Å, where the partial spin moments of Mn (A) and Mn (B) are 1.78 and −0.04 μ_B, respectively. The stable integer value of the magnetic moment is a typical character of half-metallic materials in a certain pressure range; in order to testify this further, the band structures and density of states (DOS) of Mn_2RuSi with Hg_2CuTi-type structure at 0, 50, and 100 GPa are presented in Figs. 3 and 4, respectively.

From Fig. 3, it is evident that in spin-up band structure, the valence bands overlap with conduction bands for Hg_2CuTi-type Mn_2RuSi and the Fermi level passes through

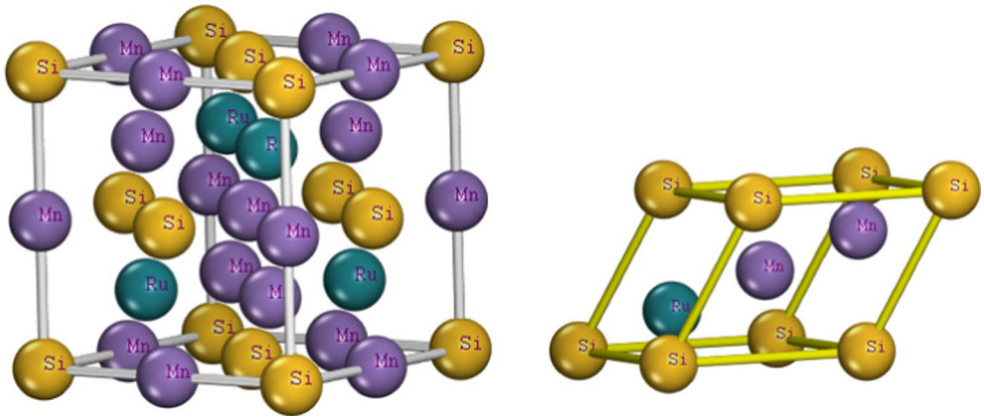

Fig. 1 Schematic representations of Mn_2RuSi with Hg_2CuTi-type structure of conventional cell (*left*) and primitive cell (*right*)

the overlapping regions. In contrast to the metallic nature of the spin-up band structures, a little gap in the spin-down band structure can be seen at zero pressure, although underestimates of the energy gap values are common to either LDA or GGA calculations. An energy gap of about 0.3 eV wide is obtained where the top of the spin-down valence bands is located at G point and the bottom of spin-down conduction bands is located at X point of the first Brillouin zone at zero pressure. The calculated total and partial DOS, as shown in Fig. 4, are in agreement with band structures and explain the band structures as well. From the variation of total DOS, we can easily see that the majority spin states in the vicinity of the Fermi level which is set at zero are almost full, whereas an energy gap exists for the minority spin channel, and thus, Mn_2RuSi alloy has a half-metallic character at zero pressure. The contribution to the total DOS around the Fermi level is mainly from the Ru 4*d*, Mn (A) and Mn (B) 3*d* electrons, and others contribute a little to it. From Fig. 4, it is clear that a change in pressure leads to a visible shift in the electronic structure. With the increase of the pressure from 0 to 100 GPa, the minority DOS of Mn_2RuSi is shifted to higher energy. It can be found that the

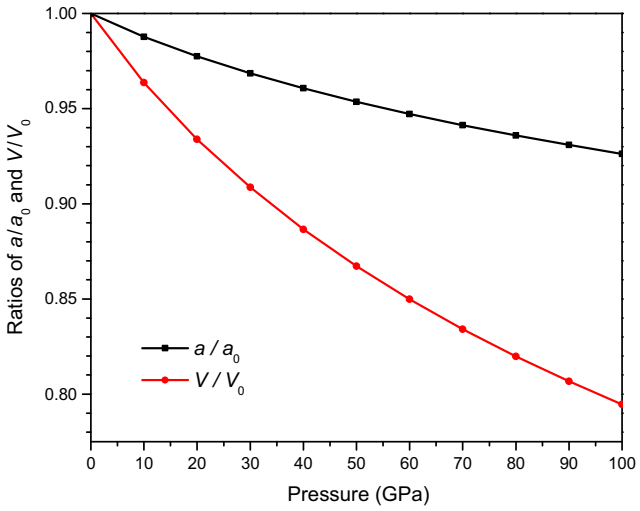

Fig. 2 Variations of the lattice constant and unit cell volume ratios for Mn_2RuSi in Hg_2CuTi-type structure with pressure

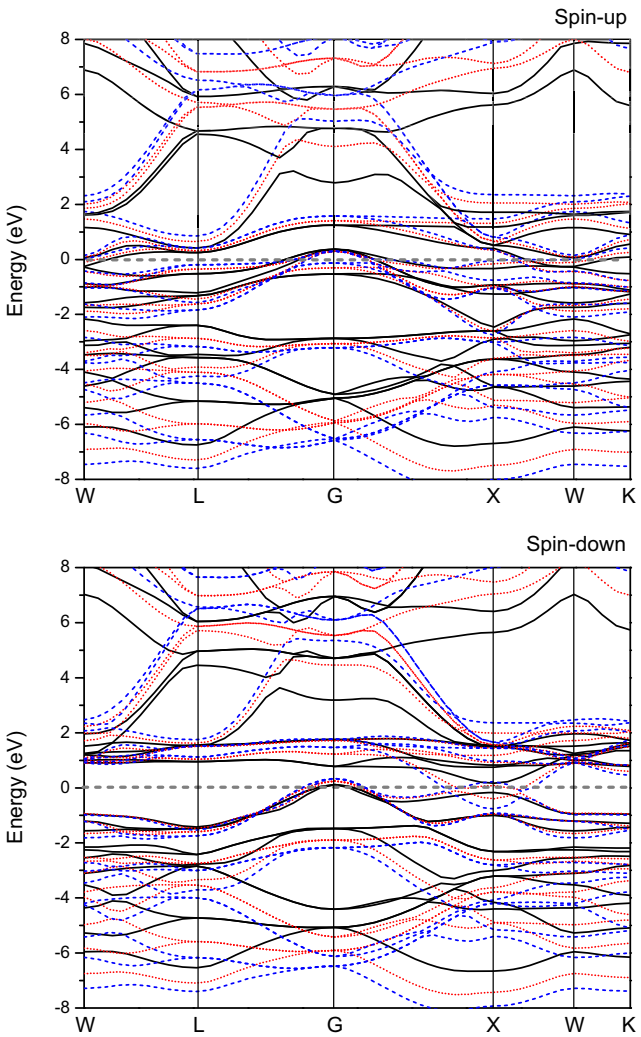

Fig. 3 The band structures of Mn_2RuSi with Hg_2CuTi-type structure for spin-up and spin-down channels at 0, 50, and 100 GPa, which are denoted by *black solid line*, *red short dot*, and *blue short dash*, respectively. The Fermi level is shown by a *horizontal gray short dash* at zero energy

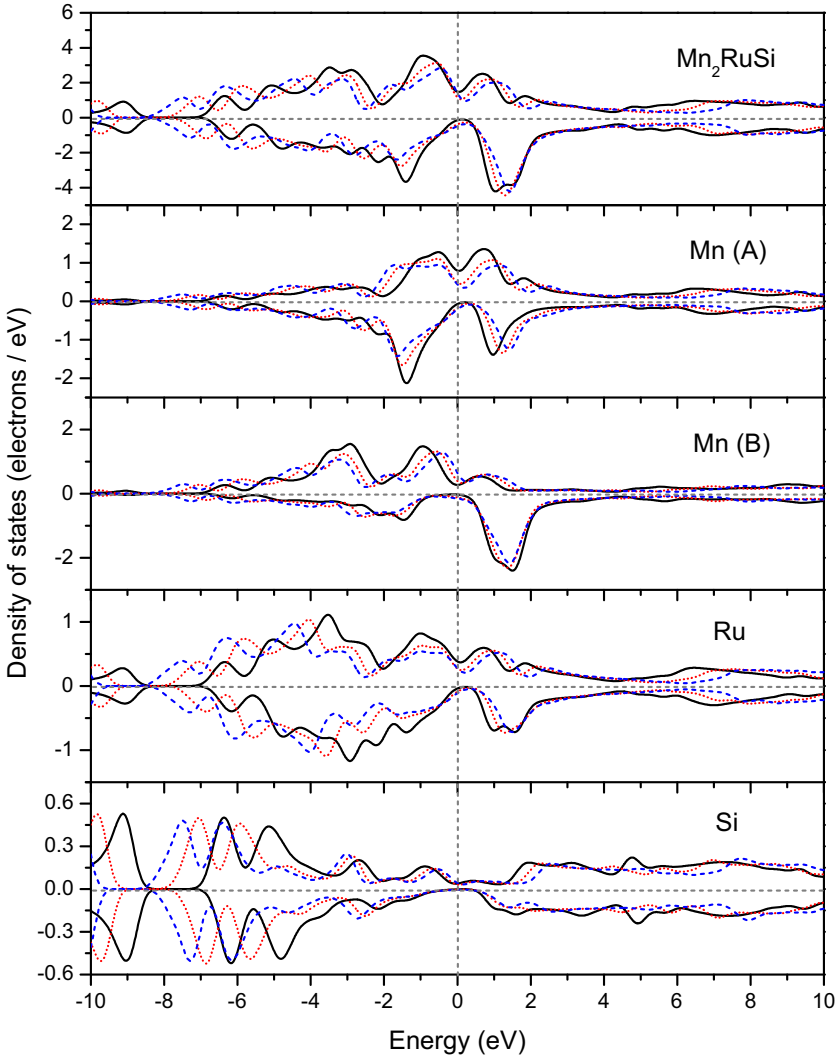

Fig. 4 The spin-projected total and partial density of states (DOS) plots for Mn_2RuSi in Hg_2CuTi-type structure at 0, 50, and 100 GPa, which are denoted by *black solid line*, *red short dot*, and *blue short dash*, respectively. The Fermi level is shown by a *vertical gray short dash* at zero energy

narrow energy gap disappears when the pressure increases up to 50 GPa.

Elastic constants under pressure are very important to determine the response of the crystal to external forces and they provide a link between the mechanical and dynamical behavior of materials. According to Ref. [32], we know that for a cubic crystal, a transverse strain leads to a change in shape with a constant volume and C_{11} changes with the longitudinal stain, where C_{12} and C_{44} characterize the elasticity in shape and C_{11}represents the elasticity in length. Figure 5 gives the pressure dependence of the three independent elastic constants for Mn_2RuSi with Hg_2CuTi-type structure at zero temperature. It is found that all of the elastic constants increase with the enhancement of pressure, and C_{44} is less sensitive to the pressure than C_{11} and C_{12}. By fitting the elastic constants, the following quadratic function relationships for the GGA calculation can be obtained:

$$C_{11} = 378.63 + 5.78P - 5.85 \times 10^{-3} P^2, \quad (13)$$

$$C_{12} = 180.95 + 4.17P - 3.05 \times 10^{-3} P^2, \quad (14)$$

$$C_{44} = 155.90 + 1.83P - 2.50 \times 10^{-3} P^2. \quad (15)$$

One of the criterions of the structural stability can be derived from the calculated elastic constants. In particular, in the case of cubic crystal, like as Mn_2RuSi in stable $F\bar{4}3m$ configuration, the conditions of stability reduce to a very simple form known as the Born stability conditions:

$$C_{11} + 2C_{12} > 0, C_{44} > 0, C_{11} - C_{12} > 0. \quad (16)$$

Under hydrostatic pressure, the generalized elastic stability criteria [33] is given by the elastic stiffness coefficients c_{ij}:

$$c_{11} + 2c_{12} > 0, c_{44} > 0, c_{11} - c_{12} > 0. \quad (17)$$

Here, the relations between C_{ij} and c_{ij} are described as follows:

$$c_{11} = C_{11}, c_{12} = C_{12} + P, c_{44} = C_{44} - \frac{P}{2}. \quad (18)$$

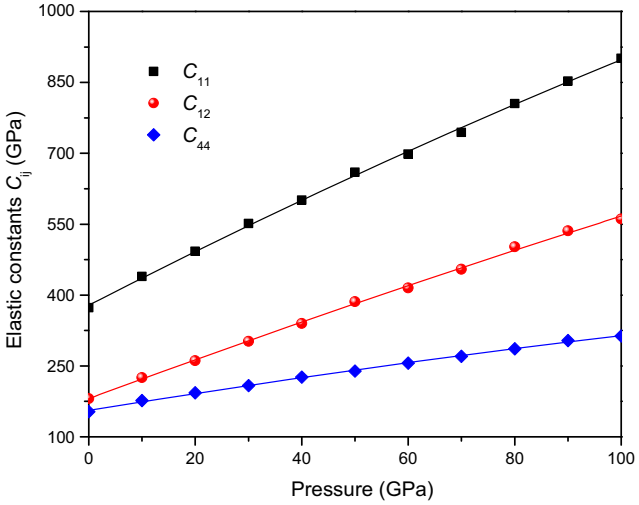

Fig. 5 The pressure dependence of the elastic constants C_{11}, C_{12}, and C_{44} for Mn_2RuSi in Hg_2CuTi-type structure

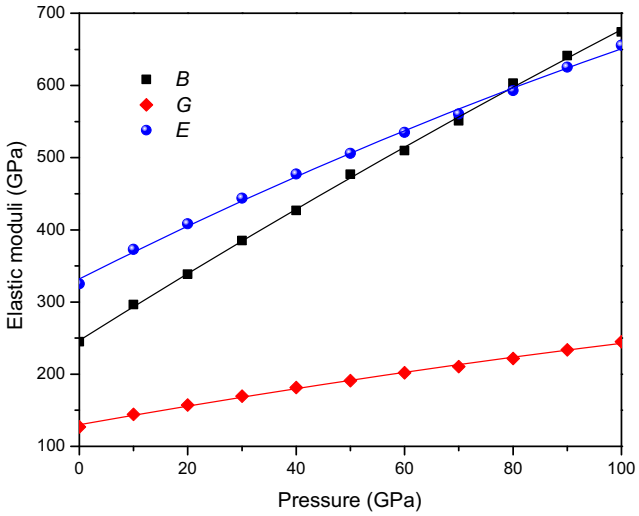

Fig. 7 The pressure dependence of the bulk, shear, and Young's moduli K, G, and E for Mn_2RuSi in Hg_2CuTi-type structure

The calculated elastic stiffness coefficients c_{ij} under high pressure for Mn_2RuSi are given in Fig. 6. It can be found from this figure that the effect of the pressure on c_{11} and c_{12} is much larger than that on c_{44} in the whole pressure range of 0–100 GPa. The c_{11} and c_{12} increase with an increment of the pressure, whereas c_{44} increases very slowly and always remains positive. These elastic stiffness coefficients fully satisfy the generalized elastic stability criteria and the prediction indicated that the cubic Mn_2RuSi alloy is stable at least 100 GPa.

In Fig. 7, we present the pressure dependence of the elastic moduli B, G, and E for Mn_2RuSi with Hg_2CuTi-type structure. As we know, the bulk modulus B and shear modulus G describe the resistance of a material to the change in volume and shape, respectively, and Young's modulus

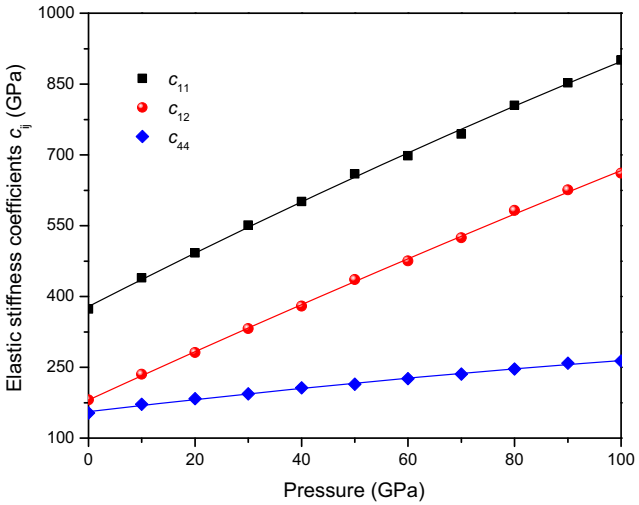

Fig. 6 The pressure dependence of the elastic stiffness coefficients c_{11}, c_{12}, and c_{44} for Mn_2RuSi in Hg_2CuTi-type structure

E describes the resistance to uniaxial tensions or compressions. We obtained bulk modulus $B = 245$ GPa, shear modulus $G = 127$ GPa, and Young's modulus $E = 325$ GPa at 0 GPa and $B = 674$, $G = 245$, and $E = 656$ GPa at 100 GPa using RVH approximations. When pressure changes from 0 to 100 GPa, bulk modulus shows a high linear increasing trend and the increasing rate is 175 %, whereas shear modulus and Young's modulus have a relatively small increasing trend and the increasing rates are 93 and 102 %, respectively, as shown in Fig. 7.

Poisson's ratio σ reflects the information and insight on the microstructure, nature and physical and mechanical properties of materials. It is usually used to quantify the stability of the crystal against shear deformation, which usually ranges from -1 to 0.5. Therefore, it deserves a special focus on after the bulk modulus B and shear modulus G obtained through (7). Pressure dependence of the Poisson's ratio for Mn_2RuSi with Hg_2CuTi-type structure is shown in Fig. 8. We can see that σ increases with increasing pressure. The bigger the σ, the better the plasticity. Furthermore, σ is larger than 1/3 for ductile materials and less than 1/3 for brittle materials. Our calculated value for σ is 0.279 at zero temperature and zero pressure, indicating that Mn_2RuSi behaves in a brittle manner. In our case, the obtained σ values are between 0.279 and 0.338 on the whole pressure range from 0 to 100 GPa for Mn_2RuSi.

Figures 9 and 10 show the dependence of the calculated velocities for average (V_m), compressional (V_p) and shear (V_s) waves, and the Debye temperature θ_D for Mn_2RuSi with Hg_2CuTi-type structure, respectively. From Fig. 9, it can be seen that the compressional wave velocity V_p increases monotonically with pressure, whereas the variational trend is not obvious for the shear wave

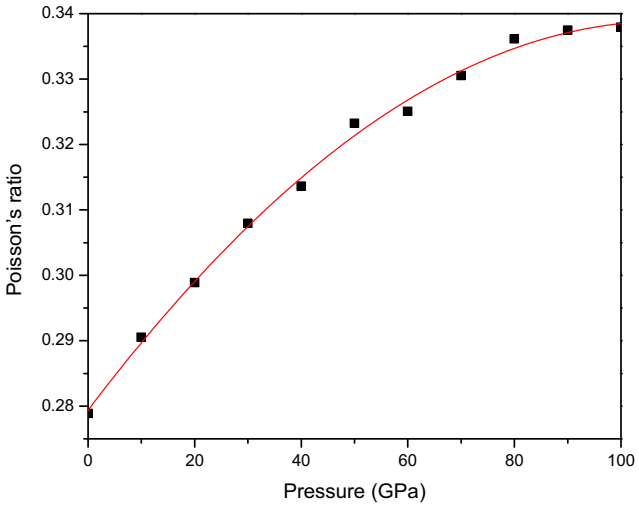

Fig. 8 The pressure dependence of the Poisson's ratio σ for Mn_2RuSi in Hg_2CuTi-type structure

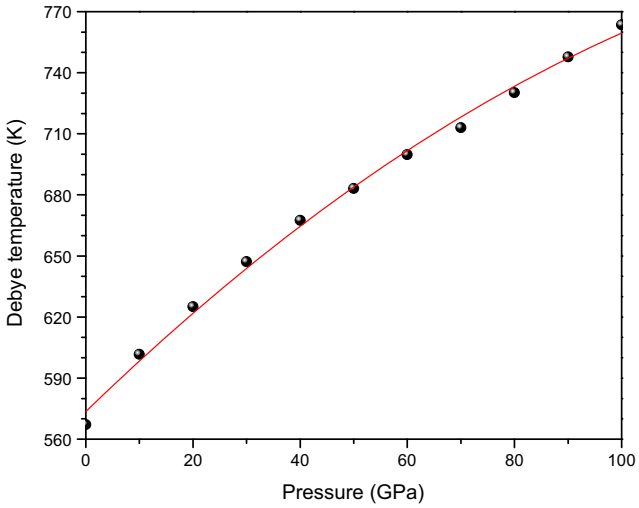

Fig. 10 The pressure dependence of the Debye temperature θ_D for Mn_2RuSi in Hg_2CuTi-type structure

velocity V_s and average elastic wave velocity V_m. It can be approximately generalized that the V_s is half of the V_p in homogenous metallic materials, that is $V_p = 2V_s$ [34] For the half-metallic Mn_2RuSi compound, the relationship between V_p and V_s is also approximately effective, especially under high pressure. The Debye temperature θ_D is related to the vibration of atoms, therefore, the high value θ_D indicates strong atomic interaction and then high value of elastic moduli of crystalline materials [28] At zero pressure and zero temperature, the Debye temperature θ_D for Mn_2RuSi is 567 K. From Fig. 10, one can see clearly that the Debye temperature increases with increasing pressure, and the lower the pressure is, the faster the Debye temperature increases.

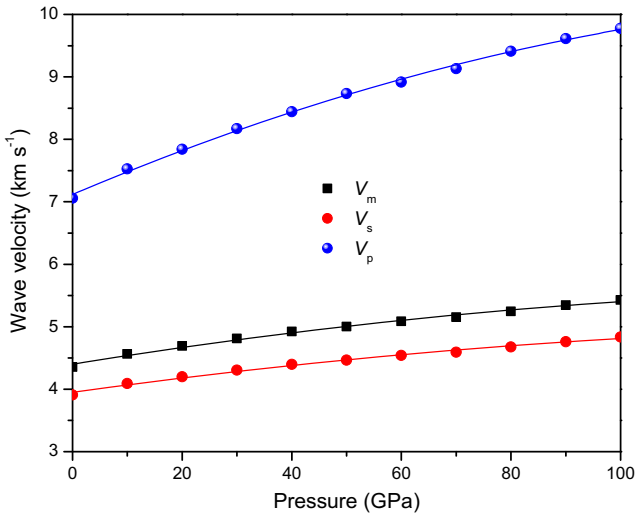

Fig. 9 The pressure dependence of the average (V_m), compressional (V_p), and shear (V_s) wave velocities for Mn_2RuSi in Hg_2CuTi-type structure

4 Conclusions

By using first-principles calculations based on density functional theory, we have studied the structural, magnetic, electronic, and elastic properties of the new Mn-based Heusler alloy Mn_2RuSi in stable $F\bar{4}3m$ configuration at high pressure. The good matching of our calculated lattice parameter with the others indicates that the present calculations are accurate. The calculated total spin magnetic moment at zero pressure is 2.01 μ_B and the partial spin moments of Mn (A) and Mn (B) which mainly contribute to the total magnetic moment are 2.48 and -0.66 μ_B, respectively. The calculations of the band structures and density of states indicate that Mn_2RuSi is a half-metallic compound with indirect band gap of 0.3 eV. When the pressure increases up to 50 GPa, the narrow energy gap is closed. The three independent elastic constants obey the necessary mechanical stability conditions and the investigation of the elastic stiffness coefficients under pressure suggesting that Mn_2RuSi is stable at least 100 GPa in Hg_2CuTi-type structure. The pressure dependence of the aggregate elastic moduli are shown that the bulk modulus shows a high linear increasing trend, whereas the shear modulus and Young's modulus have a relatively small increasing trend with increasing pressure. The calculated Poisson's ratio is 0.279 at zero temperature and zero pressure, indicating that Mn_2RuSi behaves in a brittle manner. The compressional wave velocity increases monotonically with pressure and the variational trend is not obvious for the shear wave velocity and average elastic wave velocity. For the Debye temperature the lower the pressure is, the faster the Debye temperature increases. To our knowledge, this is the first theoretical prediction of the pressure dependence of the electronic structure, phase stability, and elastic properties of inverse Heusler compound

Mn_2RuSi. We expect that our theoretical results will stimulate further experimental research on this material in the future.

Acknowledgments The authors would like to thank the support by the National Natural Science Foundation of China under Grant Nos. 11464027, 11464025, and 51562021, the Natural Science Foundation for Distinguished Young Scholars of Gansu Province under Grant No. 145RJDA323, the Program for Longyuan Youth Innovation Talents of Gansu Province, and the Colleges and Universities Scientific Research Program of Gansu Province under Grant Nos. 2015B-048 and 2015B-040.

References

1. Özdog, K., Galanakis, I.: J. Magn. Magn. Mater. **321**, L34 (2009)
2. Galanakis, I., Şaşı oğlu, E.: Appl. Phys. Lett. **99**, 052509 (2011)
3. Chakrabarti, A., Barman, S.: Appl. Phys. Lett. **94**, 161908 (2009)
4. Liu, G., Dai, X., Liu, H., Chen, J., Li, Y., Xiao, G., Wu, G.: Phys. Rev. B **77**, 014424 (2008)
5. Feng, Z., Luo, H., Wang, Y., Li, Y., Zhu, W., Wu, G., Meng, F.: Phys. Status Solidi A **207**, 1481 (2010)
6. Endo, K., Kanomata, T., Nishihara, H., Ziebeck, K.: J. Alloys Compd. **510**, 1 (2012)
7. Weht, R., Pickett, W.E.: Phys. Rev. B **60**, 13006 (1999)
8. Dai, X., Liu, G., Chen, L., Chen, J., Wu, G.: Solid State Commun. **140**, 533 (2006)
9. Luo, H., Zhu, Z., Ma, L., Xu, S., Zhu, X., Jiang, C., Xu, H., Wu, G.: J. Phys. D: Appl. Phys. **41**, 055010 (2008)
10. Luo, H., Zhang, H., Zhu, Z., Ma, L., Xu, S., Wu, G., Zhu, X., Jiang, C., Xu, H.: J. Appl. Phys. **103**, 083908 (2008)
11. Luo, H., Zhu, Z., Liu, G., Xu, S., Wu, G., Liu, H., Qu, J., Li, Y.: J. Magn. Magn. Mater. **320**, 421 (2008)
12. Wei, X.-P., Hu, X.-R., Chu, S.-B., Mao, G.-Y., Hu, L.-B., Lei, T., Deng, J.-B.: Physica B **406**, 1139 (2011)
13. Wei, X.-P., Hu, X.-R., Mao, G.-Y., Chu, S.-B., Lei, T., Hu, L.-B., Deng, J.-B.: J. Magn. Magn. Mater. **322**, 3204 (2010)
14. Luo, H., Liu, G., Meng, F., Wang, L., Liu, E., Wu, G., Zhu, X., Jiang, C.: Comp. Mater. Sci. **50**, 3119 (2011)
15. Wei, X.-P., Deng, J.-B., Chu, S.-B., Mao, G.-Y., Lei, T., Hu, X.-R.: J. Magn. Magn. Mater. **323**, 185 (2011)
16. Gupta, D.C., Bhat, I.H.: J. Alloys Compd. **575**, 292 (2013)
17. Shimosakaida, K., Fujii, S.: Mater. Trans. **57**, 312 (2016)
18. Ren, Z., Liu, Y., Li, S., Zhang, X., Liu, H.: Mater. Sci.-Poland **34**, 251 (2016)
19. Segall, M., Lindan, P.J., Probert, M.A., Pickard, C., Hasnip, P., Clark, S., Payne, M.: J. Phys.: Condens. Matter **14**, 2717 (2002)
20. Vanderbilt, D.: Phys. Rev. B **41**, 7892 (1990)
21. Perdew, J.P., Ruzsinszky, A., Csonka, G.I., Vydrov, O.A., Scuseria, G.E., Constantin, L.A., Zhou, X., Burke, K.: Phys. Rev. Lett. **100**, 136406 (2008)
22. Monkhorst, H.J., Pack, J.D.: Phys. Rev. **B13**, 5188 (1976)
23. Pulay, P.: Chem. Phys. Lett. **73**, 393 (1980)
24. Pfrommer, B.G., Côté, M., Louie, S.G., Cohen, M.L.: J. Comput. Phys. **131**, 233 (1997)
25. Fast, L., Wills, J., Johansson, B., Eriksson, O.: Phys. Rev. B **51**, 17431 (1995)
26. Voigt, W.: Ann. Phys. **38**, 573 (1889)
27. Hill, R.: Proc. Phys. Soc. Lond. A **65**, 349 (1952)
28. Reuss, A., Angew, Z.: Math. Phys. **9**, 49 (1929)
29. Schreiber, E., Anderson, O.L., Soga, N.: Elastic constants and their measurements. McGraw-Hill Companies, New York (1974)
30. Anderson, O.L.: J. Phys. Chem. Solids **24**, 909 (1963)
31. Galanakis, I., Dederichs, P., Papanikolaou, N.: Phys. Rev. B **66**, 174429 (2002)
32. Prikhodko, M., Miao, M., Lambrecht, W.R.: Phys. Rev. B **66**, 125201 (2002)
33. Wang, J., Li, J., Yip, S., Phillpot, S., Wolf, D.: Phys. Rev. B **52**, 12627 (1995)
34. Wang, W.H.: Prog. Mater. Sci. **57**, 487 (2012)